**BRIEF DEFINITIVE REPORT**

# IL-2 production by self-reactive CD4 thymocytes scales regulatory T cell generation in the thymus

Saskia Hemmers[1], Michail Schizas[1], Elham Azizi[2], Stanislav Dikiy[1,3], Yi Zhong[1], Yongqiang Feng[1], Grégoire Altan-Bonnet[4], and Alexander Y. Rudensky[1]

Regulatory T (T reg) cells, a specialized subset of CD4^{+} T cells, are essential to prevent fatal autoimmunity. Expression of the T reg lineage-defining transcription factor Foxp3, and therefore their differentiation in the thymus, is dependent upon T cell receptor (TCR) and interleukin-2 (IL-2) signaling. Here, we report that the majority of IL-2–producing cells in the thymus are mature CD4 single-positive (CD4SP) thymocytes and that continuous IL-2 production sustained thymic T reg cell generation and control of systemic immune activation. Furthermore, single-cell RNA sequencing analysis of CD4 thymocyte subsets revealed that IL-2 was expressed in self-reactive CD4SP thymocytes, which also contain T reg precursor cells. Thus, our results suggest that the thymic T reg cell pool size is scaled by a key niche factor, IL-2, produced by self-reactive CD4SP thymocytes. This IL-2–dependent scaling of thymic T reg cell generation by overall self-reactivity of a mature post-selection thymic precursor pool may likely ensure adequate control of autoimmunity.

## Introduction

Regulatory T (T reg) cells, a specialized subset of CD4^{+} T cells defined by expression of Foxp3, are critical for protection against life-threatening autoimmunity (Sakaguchi et al., 1995; Kim et al., 2007; Lahl et al., 2007). Neonatal thymectomy studies in mice demonstrated that the thymus serves as the main source of suppressive T reg cells (Asano et al., 1996). T reg cell differentiation in the thymus proceeds in a two-step fashion. Upon strong TCR stimulation by self-peptide presented on MHC class II complexes, CD4 single-positive (CD4SP) thymocytes undergo changes in gene expression, among which up-regulation of CD25, the high-affinity subunit of the IL-2 receptor, is particularly important. Induction of CD25 expression endows immediate Foxp3^{−} T reg cell precursors with the ability to effectively compete for the limiting amount of IL-2 in the thymic microenvironment (Burchill et al., 2008; Lio and Hsieh, 2008). The resulting signaling through the IL-2 receptor leading to STAT5 phosphorylation in CD25^{+}Foxp3^{−}CD4^{+} thymocytes facilitates induction and maintenance of Foxp3, the X chromosome–linked lineage-defining transcription factor, whose continuous expression is required for T reg cell differentiation and function (Burchill et al., 2007).

The size of the T reg cell population needs to be tightly controlled, to ensure suppression of autoimmunity and inflammation mediated by self-reactive T cells, while allowing for protection against microbial and abiotic challenges (Lee et al., 2012). One factor contributing to T reg cell differentiation in the thymus is the random generation of self-reactive TCRs. However, according to the two-step model, cell-intrinsic TCR signaling in T reg precursors confers potential to give rise to T reg cells, but by itself is insufficient for their differentiation. Thus, the mechanisms of scaling of the T reg cell population to the overall pool of self-reactive T cells in the thymus remains unknown.

On a general level, the size of differentiating cell populations is defined by "niche" cells, which serve as a source of a limiting key factor(s) and are frequently of a developmental origin distinct from their "client" cells. The former, by acting in a cell-extrinsic manner, affect the pool size of differentiating cells or their precursors. Considering the rather unique function of T reg cells as a dominant negative feedback to control self-reactivity, we hypothesized that contrary to a customary distinct ontogeny of niche cells, a cell-extrinsic mechanism controlling T reg population size is the limiting IL-2 produced by

self-reactive thymocytes themselves. This ensures a newly generated T reg cell population size proportional to the size of the developing self-reactive T cell pool. Here we report that a population of self-reactive CD4SP thymocytes (with a signature of recent TCR engagement) are the major source of IL-2 in the thymus that is required for efficient T reg cell differentiation and maintenance of immune homeostasis.

## Results and discussion

### Continuous dependence of thymic T reg cell generation on IL-2

Germline deficiency in IL-2 or a T reg cell–specific deletion of the IL-2 receptor subunits results in an early onset fatal autoimmunity and wasting disease, characterized by a severe reduction of T reg cells in the thymus and periphery (D'Cruz and Klein, 2005; Fontenot et al., 2005a; Chinen et al., 2016). Even though T reg cells express the high affinity IL-2 receptor (IL2Rα/CD25), they themselves do not produce IL-2 and are dependent on paracrine sources of IL-2 (Thornton and Shevach, 1998; Pan et al., 2009). Since early induction of systemic autoimmune disease including severe anemia in mice congenitally lacking IL-2 can obfuscate assessment of a role of IL-2 in T reg cell generation and does not allow its assessment in adulthood, we induced ablation of a conditional *Il2* allele (*Il2*fl) in adult mice and observed a profound decrease in the frequency of T reg cells in the thymus and effector CD4 T cell expansion and activation in the periphery (Fig. 1 A; data not shown). This observation highlighted a continuous dependence of thymic T reg cell generation on IL-2, consistent with its proposed role as a niche factor.

### IL-2–producing cells in the thymus

The cellular sources of IL-2 that promote T reg cell differentiation in the thymus and maintenance in secondary lymphoid organs or in nonlymphoid tissues have been the subject of considerable debate, and specific features of these cells remained unknown. Among candidate thymic IL-2 producers have been thymocytes, thymic dendritic cells (DCs), and stromal cells (Weist et al., 2015; Owen et al., 2018). To identify the specific cellular sources of IL-2, we generated *Il2*cre/+*Rosa26*lox-STOP-lox-Tom mice, in which cells with a developmental or "life-history" of IL-2 expression were permanently marked by a fluorescent reporter protein (tdTomato; tdTom), whose expression is induced by Cre recombinase driven by the endogenous *Il2* locus. A small percentage of cells in the thymus were tagged with tdTom (*Il2*cre–fate-mapped [FM] cells), and these cells were mostly TCRβ-expressing CD4+ thymocytes (Fig. 1, B and C; and Fig. S1 A and B). Labeled ("IL-2 fate-mapped") CD4SP thymocytes could already be detected in neonatal mice as early as postnatal day 3 (P3) and continued to increase into adulthood (Fig. 1 D, left panel). Of note, in mice at P3, the thymus was the only tissue in which labeled cells were detectable, and P3 coincided with the first T reg cells emerging from the thymus, supporting the idea that thymocyte production of IL-2 is a limiting factor for T reg cell generation. We also consistently detected FM T reg cells in the thymus, spleen, and lung of neonatal and adult mice, suggesting a life-history of IL-2 expression in precursors of some T

reg cells, even though their proportion was markedly lower than that of FM non–T reg cells (Fig. 1 D, right panel). The frequencies of labeled cells in the thymus were lower than in spleen or lung, which might be a reflection of thymic emigration during Cre-mediated recombination and expression of the fluorescent reporter or a preferential expansion of those cells in the periphery. In contrast, we failed to detect tdTom-expressing DCs or CD45⁻ stromal cells (Fig. S1 C). Consistent with these observations, ablation of a conditional *Il2* allele in DCs using a highly specific Cre driver (*Il2*Zbtb46cre/+) did not affect T reg cell development in the thymus, and the peripheral maintenance of immune homeostasis was unimpeded, ruling out thymic DCs as a source of IL-2 biologically meaningful for T reg cell generation (Fig. S1, D–F).

To assess the overall potential for stimulation-induced IL-2 protein production by different thymocyte subsets, we assayed bulk thymocytes ex vivo and detected IL-2 production by intracellular cytokine staining in CD4SP thymocytes, but to a much lesser degree in CD8SP, TCRγδ+ T cells, and natural killer T cells (Fig. 1 E). Since CD4SP thymocytes represented the major potential source of IL-2 in the thymus, we sought to more precisely define the IL-2 producers among them, specifically, by dividing them into four major subsets: thymic T reg cells (CD4+Foxp3+), CD4+CD25+Foxp3⁻ cells, and CD4+CD25⁻Foxp3⁻ cells that were further subdivided into immature and mature CD4SP cells based on CD24 and CD62L cell surface expression (for gating strategy, see Fig. S2). These four subpopulations were assessed for chromatin accessibility at the *Il2* locus measured by ATAC-seq (Assay for Transposase-Accessible Chromatin using sequencing) analysis. Strikingly, only the CD4+CD25+Foxp3⁻ subset exhibited an active *Il2* locus marked by open chromatin, suggesting that this population is enriched in cells that express IL-2, have the potential to express IL-2, or have a recent history of its expression (Fig. 1 F). We surmised that these cells may have recently received strong TCR stimulation upon self-peptide:MHC class II recognition that led to IL-2 expression and CD25 up-regulation. Indeed, in line with previously published data, we found that CD4+CD25+Foxp3⁻ cells expressed high levels of Nur77 when compared with the mature CD4SP subset, supporting the idea that this population is enriched in self-reactive T cells (Fig. 1 G; Moran et al., 2011). To further delineate the ability of these various subsets to secrete IL-2, we sorted the populations described above and stimulated them ex vivo. Immature CD4SP and thymic T reg cells expressed and secreted little IL-2. The majority of IL-2 was produced by mature CD4SP and to a lesser degree by CD4+CD25+ thymocytes (Fig. 1, H and I). These data represent the potential of all cells within each subpopulation to produce IL-2 after encountering strong TCR stimulation through PMA and ionomycin (Fig. 1 H) or TCR cross-linking (Fig. 1 I), irrespective of their TCR affinity for self-antigens, the predominant source of TCR ligands encountered by thymocytes in an unperturbed animal.

### Thymocytes, but not peripheral T cells, provide IL-2 for T reg cell generation

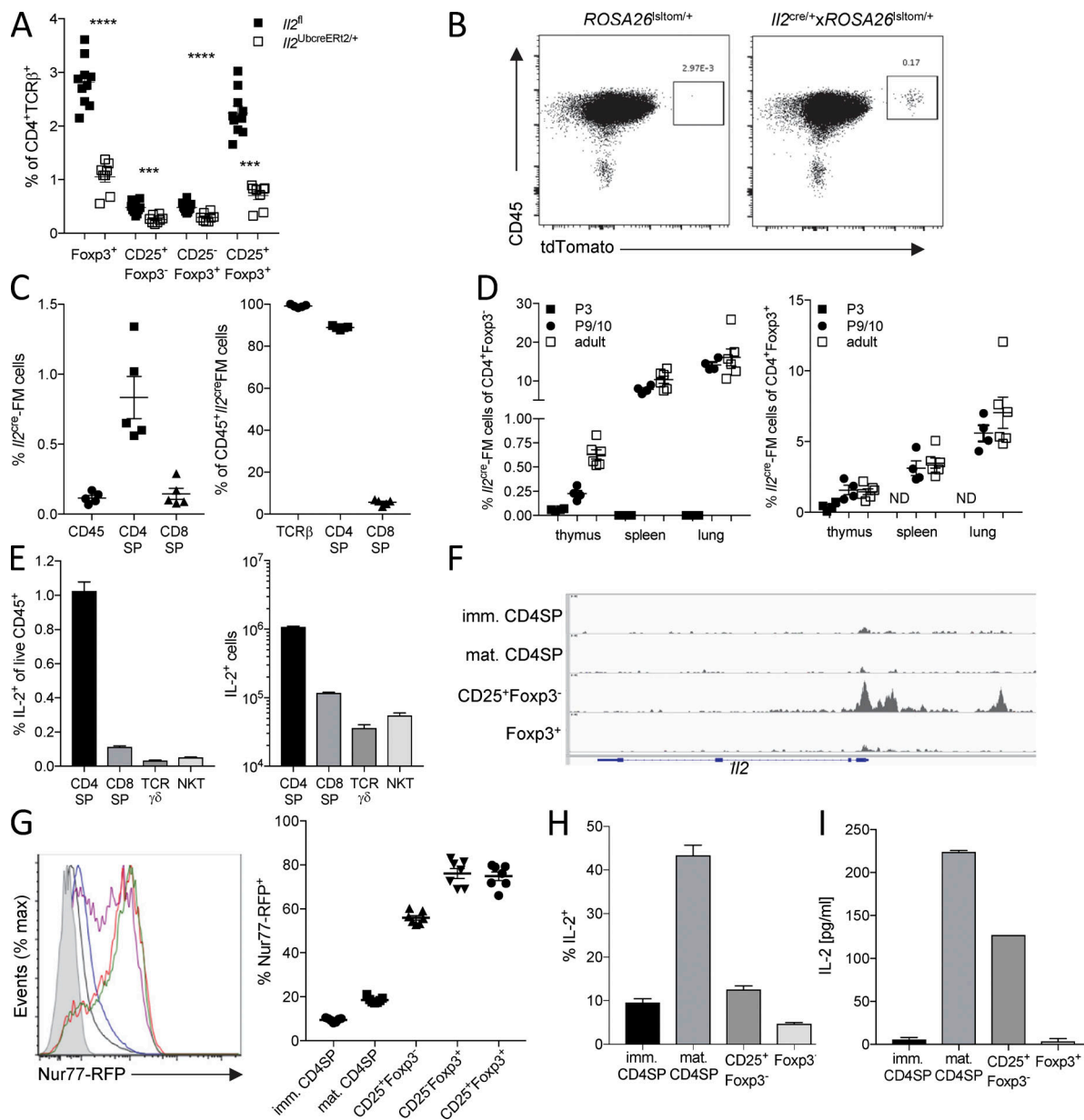To confirm the role of thymocyte-derived IL-2 in thymic T reg cell generation, we employed various genetic approaches.

Hemmers et al.
Provision of IL-2 by self-reactive CD4 thymocytes is key to T reg cell generation in the thymus

Journal of Experimental Medicine 2467
https://doi.org/10.1084/jem.20190993

Figure 1. **The majority of IL-2 producers in the thymus are self-reactive CD4SP thymocytes. (A)** Frequency of T reg cells and precursors (CD25⁺Foxp3⁻) in the thymus pregated on CD4SP thymocytes in control mice (*Il2*ᶠˡ; *n* = 10) and mice with an inducible deletion of IL-2 (*Il2*ᵁᵇᶜʳᵉᴱᴿᵗ²/⁺; *n* = 8) treated with a tamoxifen diet for 4 wk. **(B–D)** Frequency of *Il2*ᶜʳᵉ-FM cells in representative flow cytometry plots (B) and relative make-up of the FM cells in the thymus of *Il2*ᶜʳᵉ/⁺x*ROSA26*ˡˢˡᵗᵒᵐ/⁺ (*n* = 5; C) or at various stages of development: P3 (*n* = 4; black squares), P9/10 (*n* = 4; black circles), adult (*n* = 6; open squares) in thymus, spleen, or lung within CD4⁺Foxp3⁻ (left panel) or CD4⁺Foxp3⁺ (right panel; D). **(E)** Relative (left panel) and absolute (right panel) quantification of IL-2–producing thymocytes after 4 h ex vivo stimulation with PMA and ionomycin (*n* = 8). **(F)** ATAC-seq analysis of sort-purified CD4SP thymocytes; accessibility at the *Il2* locus is highlighted. Analysis was performed in duplicate, but for simplification only one track is shown per cell type. **(G)** Flow cytometry of Nur77 expression in *Nur77*ᴿᶠᴾ*Foxp3*ᴳᶠᴾ mice (*n* = 7), quantified over several mice in the right panel (shaded histogram, reporter negative; black line, immature [imm.] CD4SP; blue line, mature [mat.] CD4SP; purple line, CD25⁺Foxp3⁻; red line, CD25⁻Foxp3⁺; green line, CD25⁺Foxp3⁺). **(H and I)** IL-2 production of purified CD4SP thymocyte subsets quantified by intracellular cytokine staining after ex vivo stimulation with PMA and ionomycin for 4 h (H) or by ELISA after stimulation on αCD3/αCD28-coated plates for 12 h (I). Data in A, C–E, and G–I are means ± SEM. Data in A–C, E, and G–I represent at least three independent experiments. ****, P ≤ 0.0001; ***, P ≤ 0.001 by unpaired *t* test.

Deleting an *Il2*ᶠˡ allele in all T cells early during thymocyte differentiation using proximal Lck promoter-Cre (*Il2*ᵖᴸᶜᵏᶜʳᵉ) or CD4-Cre transgenes (data not shown) revealed a profound defect in T reg cell differentiation in the thymus (Fig. 2 A). The frequency of CD25⁺Foxp3⁻ CD4SP was unchanged, but the CD25⁺Foxp3⁺ T reg cell compartment was reduced by ~50%. Of

note, the overall frequency of Foxp3⁺ thymocytes was only slightly decreased, due to an increase in CD25⁻Foxp3⁺ thymocytes, a recently described putative T reg cell differentiation intermediate (Owen et al., 2019). This reduction of T reg cells was also evident in secondary lymphoid organs and was accompanied by increases in activated and proliferating CD4 and
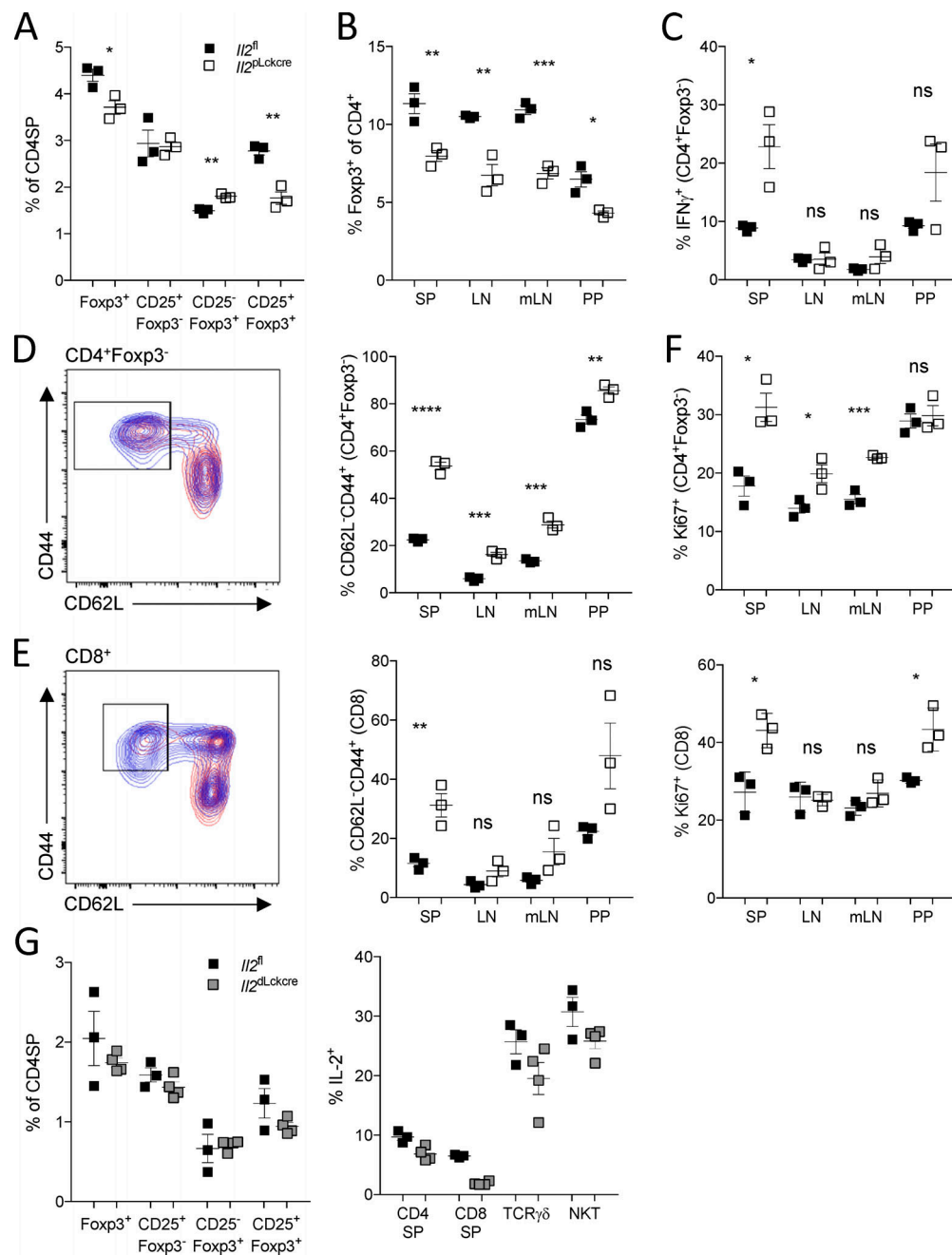
Figure 2. **Deletion of IL-2 early during T cell development impairs T reg cell development and results in immune activation in secondary lymphoid organs. (A)** Frequency of T reg cells and precursors (CD25$^+$Foxp3$^-$) in the thymus pregated on CD4SP thymocytes in 7-wk-old control mice ($Il2^{fl}$; $n = 3$; black squares) and mice with a T cell–specific deletion of IL-2 ($Il2^{pLckcre}$; $n = 3$; open squares). **(B–F)** Frequency of Foxp3-expressing T reg cells (B), IFN-γ–expressing CD4$^+$ T cells (C), activated CD62L$^-$CD44$^+$ CD4 T cells (D), CD8 T cells (E), and proliferating (Ki67$^+$) CD4 and CD8 T cells (F) in secondary lymphoid organs of the above-mentioned mice. The left panels of D and E are representative images of flow cytometry data showing an overlay of control (red) and $Il2^{pLckcre}$-derived T cells (blue) plotted in the adjacent bar graphs. **(G)** Frequency of T reg cells and precursors (CD25$^+$Foxp3$^-$) in the thymus pregated on CD4SP thymocytes in 14-wk-old control mice ($Il2^{fl}$; $n = 3$; black squares) and mice with a T cell–specific deletion of IL-2 ($Il2^{dLckcre}$) late during development ($n = 4$; gray squares; left panel) and IL-2 production of various thymic T cell populations after a 4-h ex vivo stimulation with PMA and ionomycin (right panel). All data are presented as means ± SEM and are representative of at least three independent experiments. ****, $P \leq 0.0001$; ***, $P \leq 0.001$; **, $P \leq 0.01$; *, $P \leq 0.05$; ns, $P > 0.05$ by unpaired $t$ test. PP, Peyer's patches; mLN, mesenteric LN; NKT, natural killer T cells.

CD8 T cells and elevated IFN-γ production observable already in young mice (Fig. 2, B–F). These findings raised the question whether a small number of IL-2–producing activated peripheral CD4$^+$CD25$^+$Foxp3$^-$ T cells re-enter the thymus and serve as a source of IL-2 for T reg cell differentiation. To exclude the latter possibility, we ablated IL-2 very late in thymocyte differentiation and in peripheral T cells using a distal Lck (dLck) promoter–driven Cre transgene ($Il2^{dLckcre}$). We found no discernible impact on T reg cell differentiation in the thymus (Fig. 2 G); yet peripheral T cell activation was observed, albeit

Hemmers et al.
Provision of IL-2 by self-reactive CD4 thymocytes is key to T reg cell generation in the thymus

Journal of Experimental Medicine
https://doi.org/10.1084/jem.20190993

2469

less pronounced than in *Il2*[pLckcre] mice (Fig. S3). In addition, our IL-2 fate mapping in neonatal mice described above also strongly supports a thymic origin of the IL-2 producers at the time of T reg cell emergence (Fig. 1 D). These data combined with the ATAC-seq results suggest that self-reactive CD25^{+}Foxp3^{−}CD4SP thymocytes, a subset that also contains T reg precursor cells, are the relevant source of IL-2 that promote T reg cell generation in the thymus.

## TCR-induced IL-2 production by CD4SP thymocytes promotes T reg cell generation

To explore the relationship between producers and consumers of IL-2, we set up an in vitro model of thymic T reg cell differentiation based on a two-step process requiring strong TCR stimulation followed by exposure to IL-2, leading to induction of Foxp3 expression. Both immature and mature CD4SP cells, upon stepwise TCR stimulation and exposure to IL-2, could up-regulate Foxp3 protein expression. The efficiency of Foxp3 induction scaled with the amount of IL-2 provided, and was higher with mature CD4SP as a starting population (Fig. 3 A). TCR stimulation was absolutely required for Foxp3 induction, as IL-2 alone was not sufficient to induce Foxp3 in either subset (Fig. 3 B). If starting with CD4^{+}CD25^{+} CD4SP cells, which have presumably experienced strong TCR signaling, exposure to IL-2 alone was sufficient to induce Foxp3 expression, in agreement with a previous report (Fig. 3 C; Lio and Hsieh, 2008). Exposure to conditioned media after withdrawal of TCR stimulation was sufficient to induce Foxp3 expression in mature CD4SP, and the inducing activity was reduced by ≥50% upon antibody-mediated blockade of IL-2 (Fig. 3 B). To isolate the Foxp3 expression–promoting effect of IL-2 signaling from TCR stimulation and consequent IL-2 production, we next employed stimulation with the bacterial super-antigen staphylococcal enterotoxin B (SEB), which strongly stimulates T cells expressing TCR Vβ8 chains (White et al., 1989). Expectedly, SEB preferentially induced Foxp3 expression in Vβ8-bearing T cells in a dose-dependent manner, which was strongly impaired in the presence of blocking antibodies against IL-2 (Fig. 3 D, gray bars). Up-regulation of CD25, a surrogate for TCR stimulation, was also preferentially observed in TCR Vβ8-expressing cells, but was largely unaffected when IL-2 was neutralized (data not shown). Interestingly, we consistently observed differentiation of Vβ8-negative self-reactive T cells, even if markedly less prominent (Fig. 3 D, black bars). These results suggest that IL-2 produced by Vβ8-expressing thymocytes in response to SEB stimulated Foxp3 expression in "bystander" T reg cell precursors. Similarly, treating mice with SEB led to an overall expansion of T reg cells and IL-2 FM cells in the thymus at 48 h after injection. While the majority of the increase was contributed by thymocytes receiving strong TCR stimulation through Vβ8[+] TCR chains, we observed consistent increases in Vβ5- and Vβ6-bearing T reg cells, albeit to a smaller degree (Fig. 3, E–G). Importantly, the expansion of T reg cells was blunted in *Il2*[pLckcre] mice injected with SEB (Fig. 3, H–J). These results suggest that T reg precursor cells, upon receiving a strong TCR signal, can produce IL-2, which in turn promotes their own

differentiation into T reg cells, or differentiation of thymocytes, which have received a TCR signal before paracrine IL-2 signaling.

## Single cell RNA-sequencing (scRNA-seq) analysis of IL-2 production by CD4SP thymocytes

To gain insight into characteristic features of thymocytes producing IL-2 in situ, we performed scRNA-seq analysis of mature CD25^{−}Foxp3^{−}CD4SP, CD25^{+}Foxp3^{−}, and Foxp3^{+} CD4SP thymocytes. After initial processing, a total of 11,874 individual cellular transcriptomes were analyzed using unsupervised graphical clustering and visualized using t-distributed stochastic neighbor embedding (t-SNE). The three analyzed subsets had largely distinct distribution patterns in the resulting t-SNE plots (Fig. 4 A). The cells yielded 12 distinct clusters (clusters 0–11; Fig. 4, C and D). Performing unsupervised clustering of the top 30 differentially expressed genes from each cluster revealed 7 distinct groups of similarly regulated genes (Fig. 4 E). Clusters 1, 5, and 6 contained predominantly thymic T reg cells, enriched for expression of *Foxp3*, *Il2rb*, *Izumo1r*, and *Ctla4* strongly associated with a T reg cell signature (Zemmour et al., 2018; Fig. 4, D and E, group V). Cluster 6 in particular seemed to be enriched for genes that are associated with T reg cell activation (*Ccl5*, *Maf*, *Icos*, and *Nrp1*; Fig. 4, B and E). Cluster 11 cells were defined by a strong IFN signaling signature (*Stat1*, *Ifit1*, and *Irf7*), potentially encompassing cells undergoing late stages of T cell maturation (Xing et al., 2016; Fig. 4 E, group VI). Cluster 9 cells were enriched for gene expression associated with recent TCR signaling (*Nr4a1*, *CD69*, *Rel*, and *Orai1*). These same genes were also enriched, albeit to a somewhat lesser degree, in clusters 4, 7, and 8, which contained CD25^{+}Foxp3^{−} and Foxp3^{+} cells, probably a reflection of recent TCR engagement (Fig. 4, D and E, group II).

To analyze the most significant sources of phenotypic variation in our dataset, we performed diffusion map analysis (Fig. 4 F). The first three components correlated with signatures for IL2-STAT5 signaling/T reg cell activation, apoptosis, and TCR signaling (Fig. 4, F and G). Diffusion components 1 and 3 recapitulated T reg cell differentiation in the thymus, including the need for TCR signaling to progress from the mature CD4SP stage to facilitate up-regulation of CD25 (*Il2ra*) to compete for IL-2 and subsequent STAT5-dependent induction of Foxp3 (Fig. 4, B, F, and G). The second diffusion component highlighted apoptosis, specifically in the autoreactive CD25^{+}Foxp3^{−} thymocyte population, as reflected by the heightened expression of the proapoptotic *Bcl2l11* gene, whereas most other cells expressed increased levels of the anti-apoptotic *Bcl2* gene (Fig. 4, B, F, and G). These data suggest at least three cell fates for mature CD4SP thymocytes: death by apoptosis largely restricted to a proportion of the CD4^{+}CD25^{+} thymocytes or S1PR1-mediated emigration as a CD4^{+}Foxp3^{−} or a CD4^{+}Foxp3^{+} T cell (Fig. 4 E, group VII; Matloubian et al., 2004). Within our dataset, we were able to identify 428 cells with detectable *Il2* transcript (Fig. 4 B). Their individual transcriptomes, visualized by t-SNE projection (Fig. 5 A), were enriched for genes associated with activation of the NF-κB pathway (*Nfkb1*, *Nfkbia*) likely downstream of recent TCR engagement evidenced by increased CD69 expression. This TCR signaling signature is in strong support of our assumption that
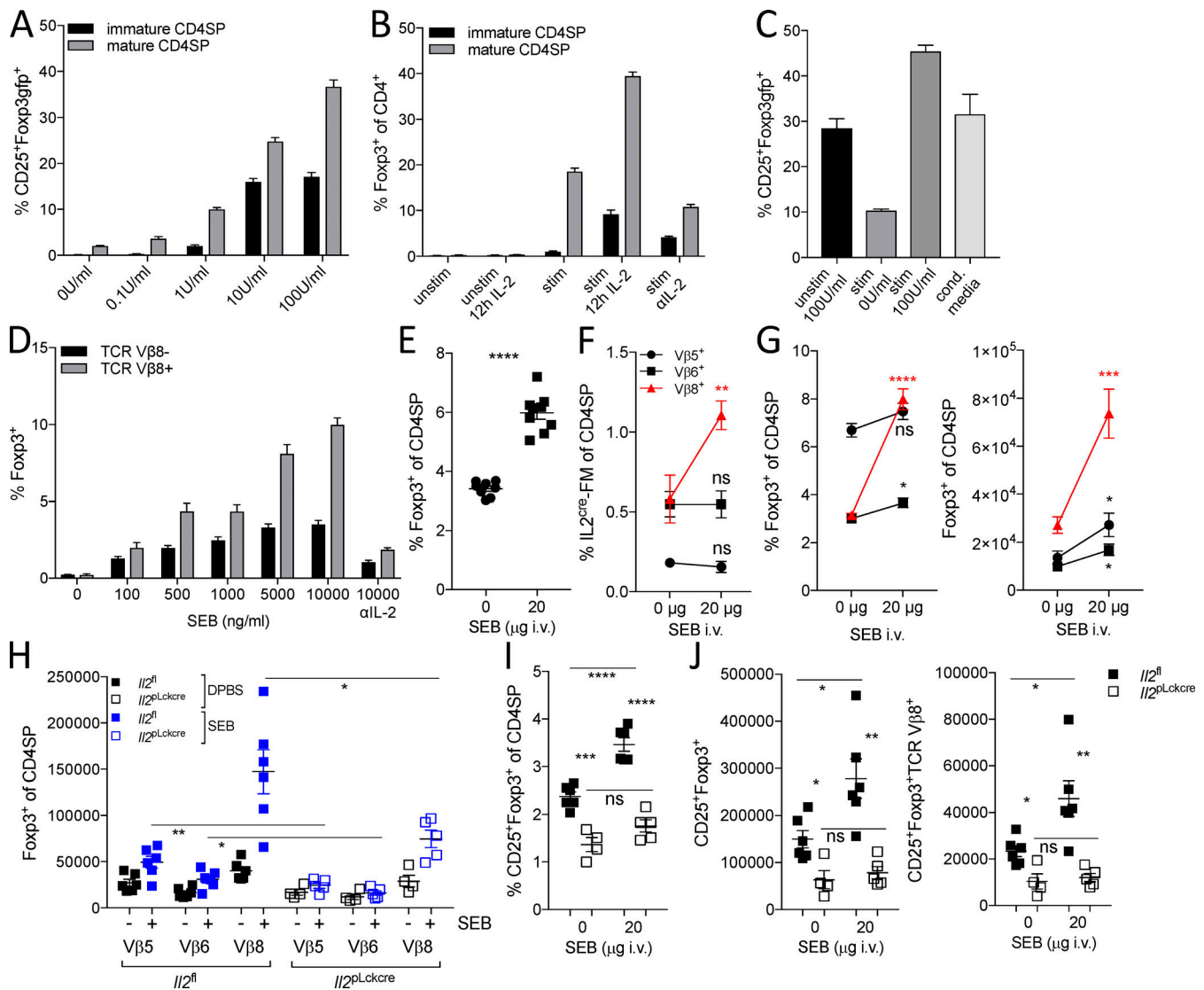
Hemmers et al.
Provision of IL-2 by self-reactive CD4 thymocytes is key to T reg cell generation in the thymus

Journal of Experimental Medicine
https://doi.org/10.1084/jem.20190993

2470

Figure 3. **SEB-mediated expansion of the thymic T reg cell compartment requires T cell–derived IL-2. (A–D)** In vitro assays to model Foxp3 induction in the thymus. Foxp3 expression was quantified by flow cytometry at the end of the assay. **(A)** Sort-purified immature (black bars) or mature (gray bars) CD4SP from three individual *Foxp3*^GFP mice were stimulated in triplicates with plate-bound αCD3 and αCD28 for 10–12 h and then replated in the presence of increasing amounts of rhIL-2 for an additional 12 h. **(B)** Immature and mature CD4SP were sort-purified and cultured in triplicates on αCD3/αCD28-coated (stim) or uncoated (unstim) plates for 10–12 h and then replated in fresh media with 100 U/ml rhIL-2 (12h IL-2) or replated in their conditioned (cond.) media with or without IL-2–blocking antibodies (αIL-2). **(C)** Similar assay set-up to B, but the starting population consisted of CD25^+Foxp3^− CD4SP thymocytes. **(D)** Mature CD4SP thymocytes were isolated from *Foxp3*^GFP mice and co-cultured with splenic DCs and increasing concentrations of SEB for 24 h. Foxp3 induction was assayed comparing TCR Vβ8^+ cells versus all other TCR Vβ–expressing thymocytes. **(E–G)** *Il2*^cre FM mice were injected with DPBS (n = 8) or 20 µg SEB (n = 9) i.v. and analyzed 48 h after treatment. **(E)** Frequency of Foxp3-expressing cells in control versus SEB-treated animals. **(F)** Frequency of *Il2*^cre-FM cells within CD4SP thymocytes expressing TCR Vβ5, TCR Vβ6, or TCR Vβ8. **(G)** Increase of Foxp3-expressing cells in SEB-treated mice plotted separately for TCR Vβ5-, TCR Vβ6-, or TCR Vβ8–expressing CD4SP thymocytes. **(H–J)** Control mice (*Il2*^fl) or mice with a T cell–specific deletion of IL-2 (*Il2*^pLckcre) were injected with DPBS (n = 6 and n = 4; black filled and open squares, respectively) or 20 µg SEB (n = 6 and n = 5; blue filled and open squares, respectively) i.v. and analyzed 48 h after treatment. **(H)** Quantification of Foxp3^+ CD4SP thymocytes expressing TCR Vβ5, Vβ6, or Vβ8. **(I)** Frequency of CD25^+Foxp3^+ CD4SP thymocytes. **(J)** Quantification of CD25^+Foxp3^+ thymocytes (left panel) or CD25^+Foxp3^+ TCR Vβ8–expressing cells (right panel). Data are plotted as means ± SEM and represent cells sorted from three individual mice (A–C) or two individual mice (D) analyzed as three technical repeats and repeated independently at least twice, pooled from three independent experiments (E–G), or pooled from two independent experiments (H–J). ****, P ≤ 0.0001; ***, P ≤ 0.001; **, P ≤ 0.01; *, P ≤ 0.05; ns, P > 0.05 by unpaired *t* test.

the IL-2 producers are enriched in the self-reactive pool of CD4SP thymocytes, since self-antigens are predominantly presented by MHC class II in the thymus of an unperturbed mouse. Consistent with a known role for NF-κB signaling in promoting survival, we observed increased Bcl2 expression, which offers

protection from TNF-mediated death, and the type I IFN pathway (*Isg15*, *Stat1*) also required for late-stage maturation of T cells in the thymus (Fig. 5, B–D; Xing et al., 2016). About a third of the cells co-expressed *Foxp3* and *Il2*, consistent with the idea that at least a fraction of IL-2–producing self-reactive precursor

Hemmers et al.
Provision of IL-2 by self-reactive CD4 thymocytes is key to T reg cell generation in the thymus

Journal of Experimental Medicine
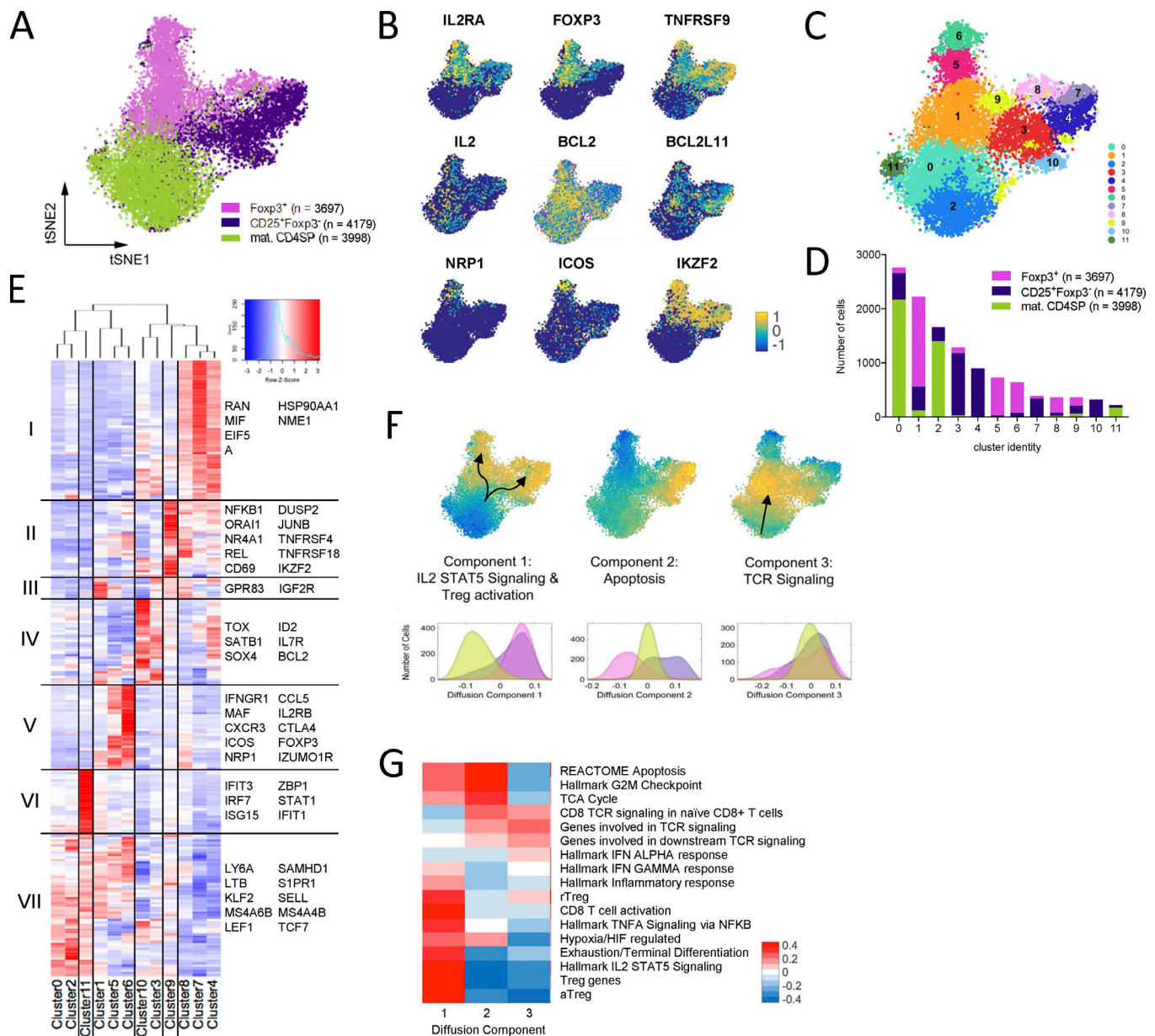https://doi.org/10.1084/jem.20190993

2471

**Figure 4. Single-cell transcriptomics of CD4SP thymocytes and their inferred developmental trajectories. (A)** t-SNE projection of library size normalized and log-transformed data for 11,874 transcriptomes profiled with scRNA-seq. Each dot represents a cell colored by input sample. **(B)** Normalized expression of selected marker genes. **(C)** t-SNE map colored by inferred clusters using PhenoGraph. **(D)** Bar graph showing number of cells from each sample in each cluster. **(E)** Heat map displaying unsupervised clustering of the normalized expression of the top 30 differentially expressed genes from each of the 12 clusters. The graph was further divided into seven groups of similar gene expression patterns (I–VII), and exemplary genes for each group are annotated. **(F)** t-SNE map colored by the top diffusion components and assigned a label derived from the most correlated gene signature shown in G. The density of cells from each input sample is plotted along each diffusion component. **(G)** Pearson correlations between each diffusion component (columns) and expression of predefined gene signatures (rows; presented in Table S1). Mat., mature; rTreg, resting T reg; aTreg, activated T reg.

cells can differentiate into thymic T reg cells and in agreement with the presence of *Il2*^cre^-FM cells within the Foxp3^+^ thymocyte and peripheral population (Fig. 5 B and 1 D). Of note, a small proportion of IL-2–expressing cells also expressed pro-apoptotic Bim (*Bcl2l11*) and the co-stimulatory receptor 4-1BB (*Tnfrsf9*), and those cells were mostly found in the CD25^+^Foxp3^−^ thymocyte population (Fig. 5 B). This observation suggests that some self-reactive thymocytes, upon TCR stimulation, produce IL-2 but then undergo apoptosis (Fig. 5, C and D). Interestingly, 4-1BB

signaling is thought to promote IL-2 production in peripheral conventional T cells by overriding T reg cell–mediated suppression, a mechanism potentially also at work in the thymus (Barsoumian et al., 2016).

In aggregate, our studies suggest that in the thymus, IL-2 was expressed predominantly by self-reactive CD4SP thymocytes, which also harbor CD25^+^Foxp3^−^ T reg precursor cells. IL-2–expressing thymocytes exhibited a gene expression pattern characteristic of TCR engagement, NF-κB signaling, and tonic

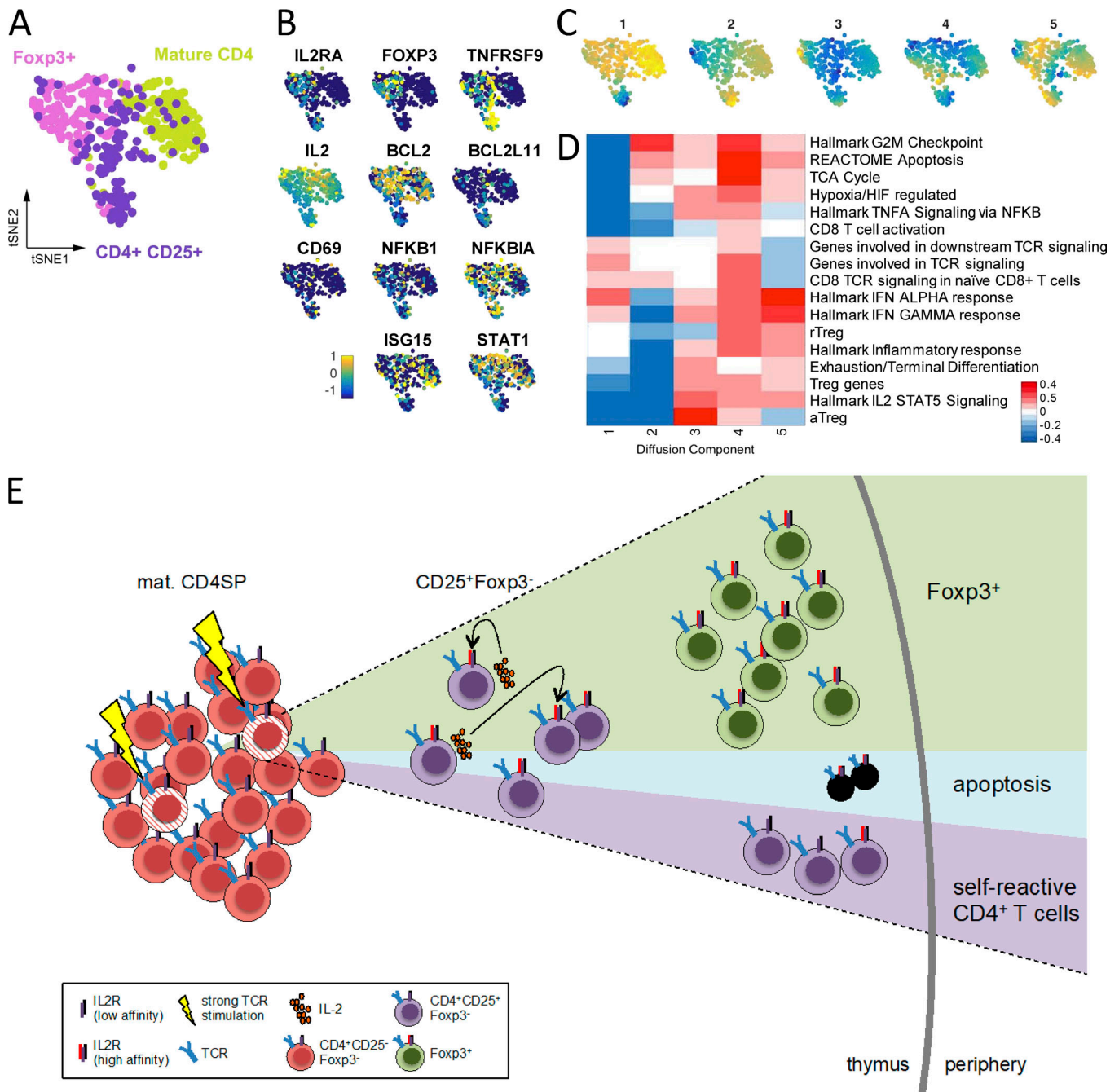Hemmers et al.
Provision of IL-2 by self-reactive CD4 thymocytes is key to T reg cell generation in the thymus

Journal of Experimental Medicine    2472
https://doi.org/10.1084/jem.20190993

Figure 5. **Unique features of *Il2*-expressing CD4SP thymocytes inferred from scRNA transcriptomics. (A)** t-SNE projection of library size normalized and log-transformed data for 428 *Il2*+ cells profiled with scRNA-seq. Each dot represents a cell colored by input sample. **(B)** Normalized expression of selected marker genes. **(C)** t-SNE map colored by the top diffusion components. **(D)** Pearson correlations between each diffusion component (columns) and expression of predefined gene signatures (rows; presented in Table S1). **(E)** A model for scaling T reg cell generation in the thymus: Self-reactive CD4SP thymocytes promote thymic T reg cell development by provision of the niche factor IL-2. Within the pool of mature CD4SP thymocytes, a small subset of self-reactive cells accounts for the majority of IL-2 production in the thymus. Expression of IL-2 induced by TCR signaling and coincident with up-regulation of CD25 is sufficient to promote T reg cell development in a paracrine and potentially autocrine fashion. The small CD25+Foxp3− pool of self-reactive thymocytes that experienced IL-2 inducing TCR stimulation is heterogeneous, with some of the cells contributing to the T reg cell lineage, some contributing to the self-reactive T cell pool, and some undergoing apoptosis. rTreg, resting T reg; aTreg, activated T reg.

type I IFN signaling and served as a key source of IL-2 for developing thymic T reg cells (Fig. 5 E). Thus, self-reactive thymocytes regulate the size of the T reg cell population generated in the thymus through production of a niche factor: IL-2.

## Materials and methods
### Mice
*Il2*fl, *Il2*cre/+, *Foxp3*GFP, and *Foxp3*Thy1.1 mice have been described previously (Fontenot et al., 2005b; Liston et al., 2008; Popmihajlov et al., 2012; Yamamoto et al., 2013). *Il2*fl mice were

Hemmers et al.
Provision of IL-2 by self-reactive CD4 thymocytes is key to T reg cell generation in the thymus

Journal of Experimental Medicine
https://doi.org/10.1084/jem.20190993

2473

provided by Vandana Kalia (University of Washington School of Medicine, Seattle, WA), *Foxp3*[GFP] and *Foxp3*[Thy1.1] were maintained in house, and the rest of the mice were obtained from The Jackson Laboratory. *Nur77*[RFP] mice were generated using the bacterial artificial chromosome (BAC) clone RP24-366J14, carrying a GFP cassette at the 5′ end of the *Nr4a1* (*Nur77*) gene, a gift from Kristin Hogquist (University of Minnesota, Minneapolis, MN; Moran et al., 2011). The GFP was replaced with the turboRFP coding sequence using standard recombineering protocols, and the *Nur77*[RFP] BAC clone was validated by PCR, Sanger sequencing, and *Spe*I digestion. Purified BAC DNA was then injected into C57BL/6J embryos, and offspring were screened for the presence of the transgene by PCR and bred to *Foxp3*[GFP] reporter mice for use in this study. *Il2*[fl] mice were used to generate *Il2*[pLckcre] mice by breeding with B6.Cg-Tg(Lck-cre)548Jxm/J, *Il2*[dLckcre] mice by breeding with B6.Cg-Tg(Lck-icre)3779Nik/J, *Il2*[Zbtb46cre/+] mice by breeding with B6.Cg-Zbtb46[tm3.1(cre)Mnz]/J, and *Il2*[UbcreERt2/+] mice by breeding with B6.Cg-Ndor1[Tg(UBC-cre/-ERT2)1EjB]/J. To induce deletion in the latter strain, mice were placed on a tamoxifen citrate–containing diet (TD.130860; Envigo) at 6–8 wk of age for 4 wk. For genetic fate mapping of IL-2–expressing cells, *Il2*[cre/+] mice were crossed with *ROSA26*[lsltom/+] mice (B6.Cg-Gt(ROSA)26Sor[tm14(CAG-tdTom)Hze]/J) and either *Foxp3*[GFP] or *Foxp3*[Thy1.1] reporter mice. All animals were maintained in the Memorial Sloan Kettering Cancer Center animal facility under specific pathogen–free conditions, and the experiments were performed according to the institutional guidelines (Institutional Animal Care and Use Committee 08-10-23). Mice aged 5–8 wk were used for all experiments unless otherwise specified in the figure legend. Mice were age matched and litter matched. Mice were sex matched when possible.

## Tissue preparation and cell isolation

For analysis of single-cell suspensions, thymus, spleen, LNs, and Peyer's patches were mechanically dissociated between frosted glass slides or with the back of a syringe plunger and filtered through a 100-µm nylon mesh. For isolation and analysis of DCs, spleen and thymus were enzymatically digested with 300 µg/ml Liberase TL (Roche) and 50 µg/ml DNaseI (Sigma-Aldrich) in RPMI-1640 for 20 min at 37°C while shaking. Splenic DCs were further enriched using magnetic CD11c MicroBeads UltraPure and LS columns (Miltenyi Biotec). For analysis of immune cells from liver, tissues were isolated after phosphate-buffered saline (DPBS) perfusion, and liver tissue was enzymatically digested with 1 mg/ml collagenase A from *Clostridium histolyticum* (Roche) and 1 U/ml DNaseI in RPMI-1640 with 2% FBS, 100 µg/ml penicillin/streptomycin, 20 mM L-glutamine, and 10 mM Hepes for 30–45 min at 37°C while shaking in the presence of three 0.25-inch ceramic spheres (MP Biomedicals). Digested tissue was filtered through 100-µm cell strainers and further enriched by 40% Percoll (GE Healthcare) centrifugation and resuspended in RPMI-10 (RPMI-1640, 10% FBS, 20 mM L-glutamine, 100 µg/ml penicillin/streptomycin, 10 mM Hepes, 1 mM sodium pyruvate, 1× MEM nonessential amino acids, and $10^{-5}$ M 2-mercaptoethanol).

To assess cytokine production after ex vivo re-stimulation, single-cell suspensions were incubated for 3–4 h at 37°C with 5% $CO_2$ in the presence of 50 ng/ml PMA and 500 ng/ml ionomycin with 1 µg/ml brefeldin A (all Sigma-Aldrich) and 2 µM monensin (BioLegend).

## Flow cytometry and antibodies

All flow cytometry data were collected on a BD LSRII (Becton Dickinson) flow cytometer or the Aurora spectral analyzer (Cytek) and analyzed using FlowJo 10.5 software (TreeStar Software). Single-cell suspensions were re-suspended in DPBS and stained with Ghost Dye Violet 510 or Ghost Dye Red 780 (Tonbo Biosciences) for dead-cell exclusion in the presence of anti-CD16/32 (Tonbo Biosciences) to block binding to Fc receptors for 10 min at 4°C. Cell-surface antigens were stained for 20 min at 4°C in FACS buffer (DPBS, 0.5% BSA, and 2 mM EDTA). Cells were analyzed unfixed, fixed with 2% paraformaldehyde (Thermo Fisher Scientific) for later analysis, or fixed and permeabilized with the BD Cytofix/Cytoperm kit (for intracellular cytokine staining) or the eBioscience Foxp3/Transcription Factor staining buffer set. Fixation, permeabilization, and intracellular staining were performed as recommended by the manufacturer. All cells were re-suspended in FACS buffer and filtered through 100-µm nylon mesh before analysis on the flow cytometer. 123count eBeads (eBioscience) were added at 5,000 beads per sample to quantify absolute cell numbers.

Antibodies used in this study were purchased from BioLegend, BD Biosciences, eBioscience, Thermo Fisher Scientific, or Tonbo Biosciences. The following clones were used: CD45 (30-F11), CD45.1 (A20), CD45.2 (104), NK1.1 (PK136), Ter-119 (Ter-119), TCRγδ (GL3), TCRβ (H57-597), TCR Vβ5.1, 5.2 (MR9-4), TCR Vβ6 (RR4-7), TCR Vβ8.1, 8.2 (KJ16-133.18), CD3ε (145-2C11), CD4 (RM4-5, GK1.5), CD8a (53–6.7), CD8b (YTS156.7.7), CD62L (MEL-14), CD44 (IM7), CD24 (M1/69), CD25 (PC61), CD90.1 (HIS51), CD90.2 (30-H12, 53–2.1), Ki67 (SolA15), B220 (RA3-6B2), CD19 (6D5, 1D3), CD11c (HL3), MHCII (I-A/I-E; M5/114.15.2), Foxp3 (FJK-16s), IFNγ (XMG1.2), and IL-2 (JES6-5H4).

## Cell sorting and in vitro T reg cell induction assays

Thymi from *Foxp3*[GFP] or *Foxp3*[Thy1.1] reporter mice were dissected and disassociated into a single-cell suspension. Cells were re-suspended in depletion buffer (DPBS, 2% FBS, and 2 mM EDTA) and enriched for CD4SP thymocytes by depleting CD8SP and double-positive cells using the Dynabeads Flowcomp mouse CD8 kit (Life Technologies). The enriched cells were stained with fluorochrome-conjugated anti-CD45, anti-TCRβ, anti-CD4, anti-CD24, anti-CD62L, and anti-CD25 and biotinylated anti-CD8, anti-TCRγδ, and anti-NK1.1 (dump gate), followed by fluorochrome-conjugated streptavidin before sorting on a BD FACSAria II sorter. The populations were sorted using gates shown in Fig. S2.

A typical in vitro T reg cell induction assay was set up with $2 \times 10^4$ to $5 \times 10^4$ cells per well of a flat-bottom 96-well tissue culture plate (in most cases immature and mature CD4SP thymocytes). The 96-well plates had been either coated with anti-CD3 and anti-CD28 at 1 µg/ml in DPBS for 12 h at 4°C or left untreated. Cells were cultured in RPMI-10 for 10–12 h in those plates and then transferred to V-bottom 96-well plates and re-suspended in fresh RPMI-10 supplemented with recombinant

Hemmers et al.
Provision of IL-2 by self-reactive CD4 thymocytes is key to T reg cell generation in the thymus

Journal of Experimental Medicine
https://doi.org/10.1084/jem.20190993

2474

human IL-2 (Roche) at the indicated concentrations or re-suspended in their own media (conditioned media) for an additional 12 h. To block the effects of IL-2, a cocktail of IL-2–blocking antibodies was added (S4B6-1, JES6-1A12; 5 µg/ml; BioXcell) throughout.

For the SEB-mediated induction of Foxp3 expression, mature CD4SP thymocytes were co-cultured with CD11c bead–enriched splenic DCs that had been further FACS purified as CD11c⁺MHCII^hi cells at a 2:1 ratio. SEB (Millipore) was added at a range of concentrations as indicated. After 12 h of culture, TCR stimulation was blocked by addition of I-A^b specific antibody Y3P (1 µg/ml), and the cells were cultured for an additional 12 h before Foxp3 protein induction was assessed.

### ELISA
Quantification of IL-2 protein levels in cell culture supernatants was performed using the Ready-SET-Go! Mouse IL-2 kit (eBioscience) according to the manufacturer's instructions. ELISAs were read at OD450 on a Synergy HTX instrument (BioTek). IL-2 levels were calculated through extrapolation from a standard curve using Prism 7 software.

### In vivo mouse treatments
For SEB treatment, mice were injected with 20 µg SEB (Millipore) or DPBS i.v. under isoflurane anesthesia and analyzed 48 h after injection.

### Statistical analysis
Graph Pad Prism (v. 7.0d) was used for all statistical analysis for biological experiments. We calculated P values by unpaired Student's $t$ test, and differences between groups were considered statistically significant with a P value cut-off of 0.05 or less. Data are represented as means ± SEM. In all cases, ****, $P \leq 0.0001$; ***, $P \leq 0.001$; **, $P \leq 0.01$; *, $P \leq 0.05$; ns, $P > 0.05$; ND, not detectable/below limit of detection.

### ATAC-seq and computational analysis
Thymi from Foxp3^GFP mice were dissociated, enriched for CD4SP cells, and stained as described above. Cells were then sorted into DNA Lo-bind tubes as follows: Foxp3-GFP⁺ CD4⁺ CD8⁻ TCRβ⁺ (Foxp3⁺), CD25⁺ Foxp3-GFP⁻ CD4⁺ CD8⁻ TCRβ⁺ (CD25⁺Foxp3⁻), CD25⁻ Foxp3-GFP⁻ CD4⁺ CD8⁻ TCRβ^hi CD24^lo (mature CD4SP), and CD25⁻ Foxp3-GFP⁻ CD4⁺ CD8⁻ TCRβ^lo CD24^hi (immature CD4SP). There were two biological replicates per cell population with 40–50,000 cells.

### Preparation of the ATAC-seq library
Immediately after sorting, cells were processed to generate ATAC libraries as previously described with minor modifications (Buenrostro et al., 2015). Briefly, cells were pelleted in a fixed-rotor mini-centrifuge at 500 ×$g$ for 5 min at 4°C. Cells were then washed in 1 ml cold PBS and pelleted again. Supernatant was aspirated, and cells were re-suspended in 50 µl ice-cold cell lysis buffer (10 mM Tris-HCl, pH 7.4; 10 mM NaCl; 3 mM MgCl$_2$; and 0.1% NP-40) to disrupt plasma membranes. Nuclei were pelleted at 1,000 ×$g$ for 10 min. Supernatant was aspirated, and nuclei were re-suspended in 50 µl transposition

reaction mixture (25 µl TD buffer; 2.5 µl TDE1; and 22.5 µl double-distilled H$_2$O; Nextera DNA sample preparation kit). Samples were incubated in a ThermoMixer at 1,100 rpm for 45 min at 42°C. DNA was then purified using a QIAGEN MinElute PCR Purification Kit, per manufacturer instructions. DNA was eluted in 10 µl buffer EB. Libraries were then barcoded and amplified with NEBNext High-Fidelity Master Mix and primers previously described (Buenrostro et al., 2013; 50 µl reaction with 10 µl DNA and 2.5 µl of 25 µM primers; one cycle of 5 min at 72°C and 30 s at 98°C; five cycles of 10 s at 98°C, 20 s at 63°C, and 1 min at 72°C). A quantitative PCR on the product determined that an additional 7 cycles (10 s at 98°C, 20 s at 63°C, and 1 min at 72°C) were required. The library was purified and size selected with Agencourt AMPure beads: 45 µl of PCR product was incubated with 18 µl of beads, and supernatant was collected (beads bound larger >2,000-bp fragments). Supernatant (63 µl) was then incubated with an additional 63 µl of beads for 5 min, supernatant was removed, beads were washed twice with 75% ethanol, and DNA was eluted into 50 µl H$_2$O by incubating for 2 min. Samples underwent quality control and quantification on an Agilent BioAnalyzer by the Integrated Genomics Operation core at Memorial Sloan Kettering Cancer Center before pooling and sequencing on an Illumina HiSeq.

### Computational analysis
Approximately 30–40 million paired-end ATAC-seq reads from different samples were aligned to the mouse reference genome assembly GRCm38 using STAR (Dobin et al., 2013). The genome was first indexed using the mode as: $STAR --runMode genomeGenerate. To align the reads, the default splicing alignment behavior was disabled. Only uniquely mapped read pairs were reserved in the output BAM files. The command for aligning the reads was as follows: $STAR --runMode alignReads --genomeLoad NoSharedMemory --readFilesCommand zcat --outSAMtype BAM SortedBy-Coordinate --outBAMcompression 6 --outFilterMultimapNmax 1 --outFilterMismatchNoverLmax 0.06 --outFilterMatchNminOverLread 0.55 --outFilterMatchNmin 30 --alignIntronMax 1 --alignEndsType Local --clip3pAdapterSeq CTGTCTCTTA. With these parameters, ~23–32 million reads were uniquely mapped to the accessible chromatin regions. After removal of duplicates by Picard (http://broadinstitute.github.io/picard/), a chromatin accessibility atlas was created using all replicates from all cell types. Briefly, ATAC-seq peaks for individual replicates were called using MACS2 (Zhang et al., 2008) using the following parameters: $macs2 callpeak -g mm -p 1e-2 --nomodel --shift 75 --extsize 200 --keep-dup all --call-summits. Reproducibility of the peaks among replicates of a cell type was evaluated as previously described (Li et al., 2011). After removing the irreproducible peaks (confidence score > 0.05), the chromatin accessibility atlas was constructed by aggregating all the reproducible peaks from the four cell types.

### scRNA-seq and computational analysis
Mature CD4⁺, CD4⁺CD25⁺Foxp3⁻, and Foxp3⁺ thymocytes were sorted from CD4SP-enriched thymocytes pooled from three Foxp3^GFP mice as described above. Cells were re-suspended at 10⁶/ml in DPBS with 0.04% BSA.

Hemmers et al.
Provision of IL-2 by self-reactive CD4 thymocytes is key to T reg cell generation in the thymus

Journal of Experimental Medicine
https://doi.org/10.1084/jem.20190993

2475

### scRNA-seq and preprocessing

Individual samples were loaded on 10X Genomics Chromium System. Libraries were prepared following 10X Genomics protocols (Chromium Single Cell 3′ Reagent Kits v2 Chemistry) and sequenced on NovaSeq 6000 (Illumina S2 flow cell, paired-end). FASTQ files were processed using the Sequence Quality Control pipeline (Azizi et al., 2018), and reads were aligned to the mouse genome mm10 from ENSEMBL GRCm38. Cells that contained a percentage of mitochondrial transcripts >5% were filtered out, resulting in 4,623 CD4+CD25+ cells, 4,151 Foxp3+ cells, and 4,548 mature CD4+ cells that passed QC metrics, with a median of 3,523 molecules/cell. Cells with total molecule counts of <1,000, determined by lower mode of distribution of total molecules per cell, were additionally filtered out to remove putative empty droplets. The resulting count matrices from all samples were then combined, resulting in a final set of 11,874 cells, and normalized to median library size, where library size is defined as total molecule counts per cell. The normalized data are then log transformed as log (0.1 + counts) for downstream analysis.

### t-SNE visualization

For dimensionality reduction and visualization of data, we further excluded genes with very low or very high expression of transcripts (log average expression <0.012 or >3 and a dispersion >0.5), and principle component analysis was performed on log-transformed normalized data. By using 30 principal components, where the number of principal components was determined by the knee-point in eigenvalues, single-cell gene expression was visualized in a two-dimensional projection with t-SNE (van der Maaten and Hinton, 2008), as shown in Fig. 4 A.

### Clustering

Clustering of cells was performed using PhenoGraph (Levine et al., 2015) and setting k = 30 nearest neighbors (Fig. 4 C). One cluster of cells was subsequently removed since it was uniformly comprised of cells with a relatively lower number of total molecules compared with other populations. Another cluster was removed because of its disparity with the rest of the data (t-SNE projected this cluster as a separate component that was comprised of cells from all three populations). Significant differentially expressed genes in each cluster were identified using a $t$ test implemented in Single-Cell Analysis in Python (Wolf et al., 2018) with default parameters. The top 30 differentially expressed genes are shown in Fig. 4 E; ribosomal genes were excluded from the heat map due to their higher capture rates in scRNA-seq.

### Diffusion component analysis

Due to the continuous structure of the data, we used diffusion maps (Coifman et al., 2005) as a nonlinear dimensionality reduction technique to find the major nonlinear components of variation across cells representing possible trajectories and gradients. We used a Gaussian kernel of perplexity = 30, symmetric Markov normalization, and t = 8 diffusion steps implemented in the tool MAGIC (van Dijk et al., 2018). Ribosomal genes were excluded in computing diffusion components. Fig. 4 F displays the top three diffusion components.

### Annotation of diffusion components

To identify processes associated with the nonlinear trajectories across cells, we computed the Pearson correlation between each diffusion component and the expression of predefined gene signatures as described elsewhere (Azizi et al., 2018). The expression of a signature is defined as the mean normalized expression across all genes listed in the signature. In addition to predefined signatures, we also included Hallmark signatures that showed significant enrichment (P < 0.05; false discovery rate < 0.1) in any of the diffusion components. This was achieved by first computing the correlation between each gene and each diffusion component, followed by ranking genes according to the correlation values and performing gene set enrichment analysis (Subramanian et al., 2005) on the preranked gene list per component. For signatures comprised of human genes, the genes were converted to their mouse orthologues. The full set of signatures used for annotation is provided in Table S1.

### Analysis of IL-2–expressing cells

For a focused analysis of IL-2–expressing cells, we selected cells with nonzero expression of *Il2* (in raw un-imputed data), achieving a subset of 428 cells that are projected using t-SNE in Fig. 5 A. Diffusion component analysis and annotation were performed independently on this subset using the same parameters as above (Fig. 5, C and D).

### Data availability

CD4SP thymocyte subset ATAC-seq and scRNA-seq data have been deposited to the Gene Expression Omnibus under accession nos. GSE134366 and GSE134902, respectively.

### Online supplemental material

Fig. S1 shows that limiting IL-2 deletion to the DC compartment has no effect on T reg cell development. Fig. S2 shows gating strategy to subset CD4SP thymocytes. Fig. S3 compares immune activation upon IL-2 deletion early or late during T cell development. Table S1 lists gene signatures used in scRNA-seq analysis.

## Acknowledgments

experiments, with the exception of the ATAC-seq experiment performed by S. Dikiy. M. Schizas and E. Azizi performed bioinformatic analyses and data visualization of the scRNA-seq data. Y. Zhong and S. Dikiy performed bioinformatic analyses and data visualization of the ATAC-seq data. Y. Feng and G. Altan-Bonnet provided unique reagents. S. Hemmers and A.Y. Rudensky wrote the manuscript with input from co-authors. A.Y. Rudensky supervised and acquired funding for the study.

# References

Asano, M., M. Toda, N. Sakaguchi, and S. Sakaguchi. 1996. Autoimmune disease as a consequence of developmental abnormality of a T cell subpopulation. *J. Exp. Med.* 184:387–396. https://doi.org/10.1084/jem.184.2.387

Azizi, E., A.J. Carr, G. Plitas, A.E. Cornish, C. Konopacki, S. Prabhakaran, J. Nainys, K. Wu, V. Kiseliovas, and M. Setty. 2018. Single-cell map of diverse immune phenotypes driven by the tumor microenvironment. *bioRxiv.* (Preprint posted April 2, 2018)https://doi.org/10.1101/221994

Barsoumian, H.B., E.S. Yolcu, and H. Shirwan. 2016. 4-1BB signaling in conventional T cells drives IL-2 production that overcomes CD4+CD25+FoxP3+ T regulatory cell suppression. *PLoS One.* 11:e0153088. https://doi.org/10.1371/journal.pone.0153088

Buenrostro, J.D., P.G. Giresi, L.C. Zaba, H.Y. Chang, and W.J. Greenleaf. 2013. Transposition of native chromatin for fast and sensitive epigenomic profiling of open chromatin, DNA-binding proteins and nucleosome position. *Nat. Methods.* 10:1213–1218. https://doi.org/10.1038/nmeth.2688

Buenrostro, J.D., B. Wu, H.Y. Chang, and W.J. Greenleaf. 2015. ATAC-seq: A method for assaying chromatin accessibility genome-wide. *Curr. Protoc. Mol. Biol.* 109:1–9. https://doi.org/10.1002/0471142727.mb2129s109

Burchill, M.A., J. Yang, C. Vogtenhuber, B.R. Blazar, and M.A. Farrar. 2007. IL-2 receptor β-dependent STAT5 activation is required for the development of Foxp3+ regulatory T cells. *J. Immunol.* 178:280–290. https://doi.org/10.4049/jimmunol.178.1.280

Burchill, M.A., J. Yang, K.B. Vang, J.J. Moon, H.H. Chu, C.W. Lio, A.L. Vegoe, C.S. Hsieh, M.K. Jenkins, and M.A. Farrar. 2008. Linked T cell receptor and cytokine signaling govern the development of the regulatory T cell repertoire. *Immunity.* 28:112–121. https://doi.org/10.1016/j.immuni.2007.11.022

Chinen, T., A.K. Kannan, A.G. Levine, X. Fan, U. Klein, Y. Zheng, G. Gasteiger, Y. Feng, J.D. Fontenot, and A.Y. Rudensky. 2016. An essential role for the IL-2 receptor in T_reg cell function. *Nat. Immunol.* 17:1322–1333. https://doi.org/10.1038/ni.3540

Coifman, R.R., S. Lafon, A.B. Lee, M. Maggioni, B. Nadler, F. Warner, and S.W. Zucker. 2005. Geometric diffusions as a tool for harmonic analysis and structure definition of data: diffusion maps. *Proc. Natl. Acad. Sci. USA.* 102:7426–7431. https://doi.org/10.1073/pnas.0500334102

D'Cruz, L.M., and L. Klein. 2005. Development and function of agonist-induced CD25+Foxp3+ regulatory T cells in the absence of interleukin 2 signaling. *Nat. Immunol.* 6:1152–1159. https://doi.org/10.1038/ni1264

Dobin, A., C.A. Davis, F. Schlesinger, J. Drenkow, C. Zaleski, S. Jha, P. Batut, M. Chaisson, and T.R. Gingeras. 2013. STAR: ultrafast universal RNA-seq aligner. *Bioinformatics.* 29:15–21. https://doi.org/10.1093/bioinformatics/bts635

Fontenot, J.D., J.P. Rasmussen, M.A. Gavin, and A.Y. Rudensky. 2005a. A function for interleukin 2 in Foxp3-expressing regulatory T cells. *Nat. Immunol.* 6:1142–1151. https://doi.org/10.1038/ni1263

Fontenot, J.D., J.P. Rasmussen, L.M. Williams, J.L. Dooley, A.G. Farr, and A.Y. Rudensky. 2005b. Regulatory T cell lineage specification by the forkhead transcription factor foxp3. *Immunity.* 22:329–341. https://doi.org/10.1016/j.immuni.2005.01.016

Kim, J.M., J.P. Rasmussen, and A.Y. Rudensky. 2007. Regulatory T cells prevent catastrophic autoimmunity throughout the lifespan of mice. *Nat. Immunol.* 8:191–197. https://doi.org/10.1038/ni1428

Lahl, K., C. Loddenkemper, C. Drouin, J. Freyer, J. Arnason, G. Eberl, A. Hamann, H. Wagner, J. Huehn, and T. Sparwasser. 2007. Selective depletion of Foxp3+ regulatory T cells induces a scurfy-like disease. *J. Exp. Med.* 204:57–63. https://doi.org/10.1084/jem.20061852

Lee, H.M., J.L. Bautista, J. Scott-Browne, J.F. Mohan, and C.S. Hsieh. 2012. A broad range of self-reactivity drives thymic regulatory T cell selection to limit responses to self. *Immunity.* 37:475–486. https://doi.org/10.1016/j.immuni.2012.07.009

Levine, J.H., E.F. Simonds, S.C. Bendall, K.L. Davis, A.D. Amir, M.D. Tadmor, O. Litvin, H.G. Fienberg, A. Jager, E.R. Zunder, et al. 2015. Data-driven phenotypic dissection of AML reveals progenitor-like cells that correlate with prognosis. *Cell.* 162:184–197. https://doi.org/10.1016/j.cell.2015.05.047

Li, Q.H., J.B. Brown, H.Y. Huang, and P.J. Bickel. 2011. Measuring reproducibility of high-throughput experiments. *Ann. Appl. Stat.* 5:1752–1779. https://doi.org/10.1214/11-AOAS466

Lio, C.W., and C.S. Hsieh. 2008. A two-step process for thymic regulatory T cell development. *Immunity.* 28:100–111. https://doi.org/10.1016/j.immuni.2007.11.021

Liston, A., K.M. Nutsch, A.G. Farr, J.M. Lund, J.P. Rasmussen, P.A. Koni, and A.Y. Rudensky. 2008. Differentiation of regulatory Foxp3+ T cells in the thymic cortex. *Proc. Natl. Acad. Sci. USA.* 105:11903–11908. https://doi.org/10.1073/pnas.0801506105

Matloubian, M., C.G. Lo, G. Cinamon, M.J. Lesneski, Y. Xu, V. Brinkmann, M.L. Allende, R.L. Proia, and J.G. Cyster. 2004. Lymphocyte egress from thymus and peripheral lymphoid organs is dependent on S1P receptor 1. *Nature.* 427:355–360. https://doi.org/10.1038/nature02284

Moran, A.E., K.L. Holzapfel, Y. Xing, N.R. Cunningham, J.S. Maltzman, J. Punt, and K.A. Hogquist. 2011. T cell receptor signal strength in Treg and iNKT cell development demonstrated by a novel fluorescent reporter mouse. *J. Exp. Med.* 208:1279–1289. https://doi.org/10.1084/jem.20110308

Owen, D.L., S.A. Mahmud, K.B. Vang, R.M. Kelly, B.R. Blazar, K.A. Smith, and M.A. Farrar. 2018. Identification of cellular sources of IL-2 needed for regulatory T cell development and homeostasis. *J. Immunol.* 200:3926–3933. https://doi.org/10.4049/jimmunol.1800097

Owen, D.L., S.A. Mahmud, L.E. Sjaastad, J.B. Williams, J.A. Spanier, D.R. Simeonov, R. Ruscher, W. Huang, I. Proekt, C.N. Miller, et al. 2019. Thymic regulatory T cells arise via two distinct developmental programs. *Nat. Immunol.* 20:195–205. https://doi.org/10.1038/s41590-018-0289-6

Pan, F., H. Yu, E.V. Dang, J. Barbi, X. Pan, J.F. Grosso, D. Jinasena, S.M. Sharma, E.M. McCadden, D. Getnet, et al. 2009. Eos mediates Foxp3-dependent gene silencing in CD4+ regulatory T cells. *Science.* 325:1142–1146. https://doi.org/10.1126/science.1176077

Popmihajlov, Z., D. Xu, H. Morgan, Z. Milligan, and K.A. Smith. 2012. Conditional IL-2 gene deletion: consequences for T cell proliferation. *Front. Immunol.* 3:102. https://doi.org/10.3389/fimmu.2012.00102

Sakaguchi, S., N. Sakaguchi, M. Asano, M. Itoh, and M. Toda. 1995. Immunologic self-tolerance maintained by activated T cells expressing IL-2 receptor alpha-chains (CD25). Breakdown of a single mechanism of self-tolerance causes various autoimmune diseases. *J. Immunol.* 155:1151–1164.

Subramanian, A., P. Tamayo, V.K. Mootha, S. Mukherjee, B.L. Ebert, M.A. Gillette, A. Paulovich, S.L. Pomeroy, T.R. Golub, E.S. Lander, and J.P. Mesirov. 2005. Gene set enrichment analysis: a knowledge-based approach for interpreting genome-wide expression profiles. *Proc. Natl. Acad. Sci. USA.* 102:15545–15550. https://doi.org/10.1073/pnas.0506580102

Thornton, A.M., and E.M. Shevach. 1998. CD4+CD25+ immunoregulatory T cells suppress polyclonal T cell activation in vitro by inhibiting interleukin 2 production. *J. Exp. Med.* 188:287–296. https://doi.org/10.1084/jem.188.2.287

van der Maaten, L., and G. Hinton. 2008. Visualizing data using t-SNE. *J. Mach. Learn. Res.* 9:2579–2605.

van Dijk, D., R. Sharma, J. Nainys, K. Yim, P. Kathail, A.J. Carr, C. Burdziak, K.R. Moon, C.L. Chaffer, D. Pattabiraman, et al. 2018. Recovering gene interactions from single-cell data using data diffusion. *Cell.* 174:716–729.e27. https://doi.org/10.1016/j.cell.2018.05.061

Weist, B.M., N. Kurd, J. Boussier, S.W. Chan, and E.A. Robey. 2015. Thymic regulatory T cell niche size is dictated by limiting IL-2 from antigen-bearing dendritic cells and feedback competition. *Nat. Immunol.* 16:635–641. https://doi.org/10.1038/ni.3171

White, J., A. Herman, A.M. Pullen, R. Kubo, J.W. Kappler, and P. Marrack. 1989. The V β-specific superantigen staphylococcal enterotoxin B:

stimulation of mature T cells and clonal deletion in neonatal mice. *Cell.* 56:27–35. https://doi.org/10.1016/0092-8674(89)90980-X

Wolf, F.A., P. Angerer, and F.J. Theis. 2018. SCANPY: large-scale single-cell gene expression data analysis. *Genome Biol.* 19:15. https://doi.org/10.1186/s13059-017-1382-0

Xing, Y., X. Wang, S.C. Jameson, and K.A. Hogquist. 2016. Late stages of T cell maturation in the thymus involve NF-κB and tonic type I interferon signaling. *Nat. Immunol.* 17:565–573. https://doi.org/10.1038/ni.3419

Yamamoto, M., Y. Seki, K. Iwai, I. Ko, A. Martin, N. Tsuji, S. Miyagawa, R.B. Love, and M. Iwashima. 2013. Ontogeny and localization of the cells produce IL-2 in healthy animals. *Cytokine.* 61:831–841. https://doi.org/10.1016/j.cyto.2012.11.026

Zemmour, D., R. Zilionis, E. Kiner, A.M. Klein, D. Mathis, and C. Benoist. 2018. Single-cell gene expression reveals a landscape of regulatory T cell phenotypes shaped by the TCR. *Nat. Immunol.* 19:291–301. https://doi.org/10.1038/s41590-018-0051-0

Zhang, Y., T. Liu, C.A. Meyer, J. Eeckhoute, D.S. Johnson, B.E. Bernstein, C. Nusbaum, R.M. Myers, M. Brown, W. Li, and X.S. Liu. 2008. Model-based analysis of ChIP-Seq (MACS). *Genome Biol.* 9:R137. https://doi.org/10.1186/gb-2008-9-9-r137